Carbohydrate Research, 230 (1992) 41–61
Elsevier Science Publishers B.V., Amsterdam

A ^{1}H-NMR and MD study of intramolecular hydrogen bonds in methyl β-cellobioside

Bas R. Leeflang [a], Johannes F.G. Vliegenthart [a], Loes M.J. Kroon-Batenburg [b], Bouke P. van Eijck [b], and Jan Kroon [b]

[a] *Department of Bio-organic Chemistry, Bijvoet Center, Utrecht University, P.O. Box 80.075, NL-3508 TB Utrecht (Netherlands)*
[b] *Department of Crystal and Structural Chemistry, Bijvoet Center, Utrecht University, P.O. Box 80.075, NL-3508 TB Utrecht (Netherlands)*

(Received September 28th, 1991; accepted January 4th, 1992)

ABSTRACT

The existence of an HO-3 · · · O-5′ intramolecular hydrogen bond in methyl β-cellobioside in solution in Me_2SO-d_6 and H_2O–CD_3OD (4:1 w/w) was studied by 500-MHz ^{1}H-NMR spectroscopy and MD simulations. Temperature coefficients for the chemical shift of the hydroxyl resonances in these solvents were determined and the rates of proton exchange in the latter solvent were obtained from NOE data. With H_2O–CD_3OD as the solvent, the HO-3 · · · O-5′ hydrogen bond was insignificant, but its presence in Me_2SO-d_6 was confirmed.

INTRODUCTION

There are several polymorphs of cellulose, with native cellulose (cellulose I) and mercerised cellulose (alkali-treated cellulose I or cellulose II) as the most common forms[1]. The conformations for celluloses I and II obtained from fibre X-ray diffraction data[2,3] are shown in Fig. 1. The hydroxymethyl groups of cellulose I are in the *tg* conformation, with O-5,6 *trans*, whereas, in cellulose II, the conformation is *gt*. An HO-3 · · · O-5′ intramolecular hydrogen bond parallel to the glycosidic bond causes each cellulose to have extended and rigid chains. As a consequence of the different conformations of the hydroxymethyl group, cellulose I also has a second intramolecular hydrogen bond (HO-2′ · · · O-6) along the chain axis that does not exist in cellulose II. Molecular mechanics (MM) calculations showed[4–6] that the latter intramolecular hydrogen bond accounts for the difference in elastic modulus between cellulose I and II, a property related to the macroscopic tensile

Correspondence to: Professor J.F.G. Vliegenthart, Department of Bio-organic Chemistry, Bijvoet Center, Utrecht University, P.O. Box 8.075, NL-3508 TB Utrecht, Netherlands

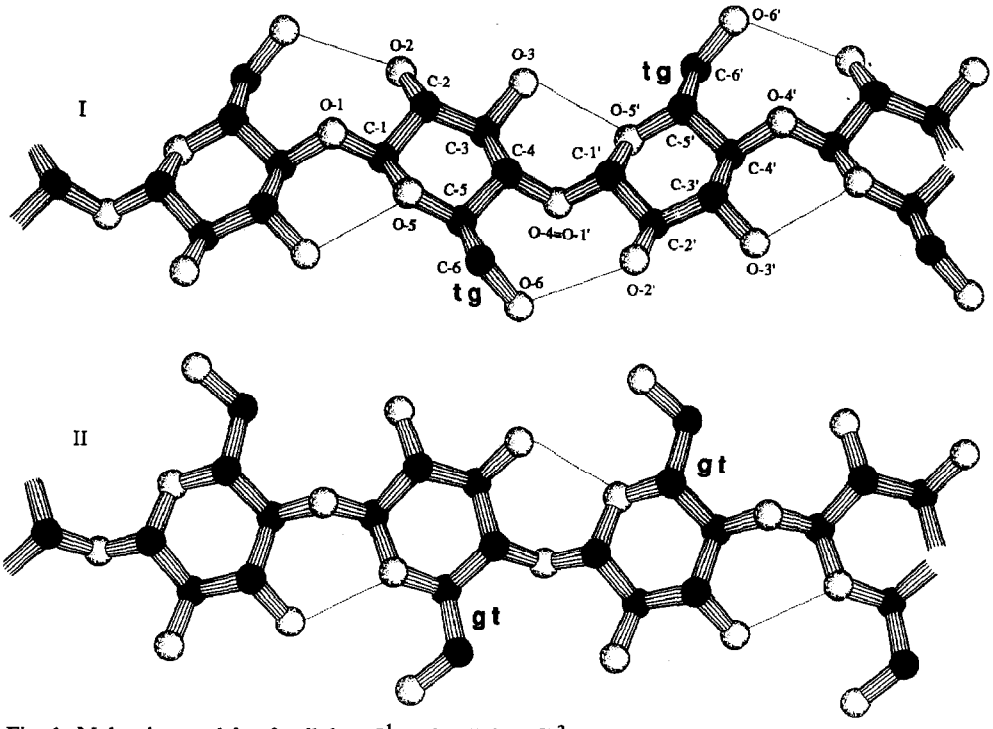

Fig. 1. Molecular models of cellulose I[1] and cellulose II[2]. The conformations of the hydroxymethyl groups are marked *tg* or *gt*, and ··· indicate intramolecular hydrogen bonds. Interglycosidic torsion angles are defined as follows: ϕ O-5–C-1–O-4–C-4, ψ C-1–O-4–C-4–C-3, ω C-4–C-5–C-6–O-6.

strength. The importance of strong fibres makes it worthwhile to study hydrogen bonding in cellulose. Because of the insolubility of cellulose in most common solvents, cello-oligosaccharides are being studied as model compounds by ^{1}H-NMR spectroscopy and molecular dynamics (MD). We now report on intramolecular hydrogen bonding in methyl β-cellobioside; cellobiose is the crystallographic repeating unit of cellulose and the methyl glycoside was studied in order to prevent anomerisation which complicates the NMR spectra.

^{1}H-NMR spectroscopy provides four parameters for the exchangeable protons of hydroxyl groups that can be used to study intramolecular hydrogen bonding: (*i*) the chemical shift δ, (*ii*) its temperature coefficient $d\delta/dT$, (*iii*) the vicinal coupling constant $^3J_{HO,CH}$, and (*iv*) the rate of exchange (k_{ex}) with the solvent. The resonances of hydroxyl protons involved in hydrogen bonds tend to be shifted downfield, but are subject to numerous effects that are hard to predict. Therefore, conclusions about conformation or hydrogen bonding based on ^{1}H chemical shift data are unreliable. However, the $d\delta/dT$ values provide information about intramolecular hydrogen bonding. The chemical shifts of the resonances of intramolecularly hydrogen-bonded hydroxyl groups and aliphatic protons show little change with temperature, because the interaction with the solvent is small and,

presumably, the conformation of the molecule is not greatly affected. However, the chemical shifts of hydroxyl protons hydrogen-bonded to the solvent have a marked temperature dependence, due to changes in mobility of the solvent molecules. Temperature coefficients < 3 ppb/deg have been measured for intramolecularly hydrogen-bonded protons. Such small $d\delta/dT$ values have been observed for amylose[7], cellulose[8], and methyl β-chitobioside[9]. The $^3J_{HO,CH}$ values are mainly dependent on the torsional angle θ of the H–O–C–H part that can be described by an empirical Karplus-type equation[10] which yields values in the range 0.2–12.1 Hz. However, it is generally not possible to calculate θ from the observed coupling constants, because they may be time averages for several conformations. The use of k_{ex} data for hydroxyl protons is limited to solvent systems that allow proton exchange. Exchange rates can be determined normally by 2D NOE spectroscopy (NOESY) by utilising a suitable suppression of the water resonance. The k_{ex} values cannot always be determined uniquely, due to spectral overlap with another hydroxyl proton. The NOHOSS technique[11], however, allows observation of exchange effects between a hydroxyl proton and water at the frequency of a 3rd proton, to which it is coupled. In order to quantify k_{ex}, corrections have to be applied to the measured NOHOSS peak intensities (see below).

With MD simulations of methyl β-cellobioside in aqueous solution, the formation of intramolecular hydrogen bonds can be studied by counting the number of time steps in which the O–H $\cdots$ O bond exists, using geometrical criteria. Since NMR data do not provide a direct measurement of the O–H $\cdots$ O interaction, additional structural parameters obtained from MD simulations can assess the significance of the experimental data [(*i*)–(*iv*) above] with respect to hydrogen bonding. The following parameters will be considered for each hydroxyl group. (*a*) The donor and acceptor capacity determined on the basis of geometrical criteria (O–H $\cdots$ $O_{intra} < 2.4$ Å) and expressed in fractions of time. (*b*) The radial distribution functions of O–H $\cdots$ O interactions within the primary solvation, which provide a measure of the interaction of a hydroxyl group with water molecules. (*c*) The accessible surface of the solvent. (*d*) The average interaction energy of a hydroxyl group with water. (*e*) The residence time of water molecules in the 1st solvation shell (see below) determined from a time-correlation function. (*f*) The average time spent by a water molecule in the 1st solvation shell of each hydroxyl group and the number of different water molecules visiting this shell. (*g*) The number of times that water molecules pass the boundary of the 1st solvation shell. The parameters (*e*)–(*g*) are dynamic and are not a direct measure of the interaction with the solvent. Most of these parameters are based on the definition of the primary solvation (see *Computational details of MD data*), in which the solvent molecules are subdivided in sections of space that belong to a particular solute atom. The correlation of the parameters (*a*)–(*g*) with the experimental data (*i*)–(*iv*) has been investigated. Although the effect of temperature on the chemical shift and the exchange process have not been simulated, it is expected that the underlying physical effects are reflected in these parameters to a certain extent.

Further, it is assumed that the solvent systems H_2O and 4:1 (w/w) H_2O–CD_3OD are sufficiently similar to allow comparisons to be made between the theoretical and experimental data, because methanol is also a hydrogen bond donor and acceptor.

EXPERIMENTAL

Materials.—Methyl β-D-glucopyranoside (**1**) and methyl β-cellobioside (**2**) were commercial products and ($^2H_3$)methyl β-cellobioside (**3**) was prepared as follows. A solution of cellobiose (327 mg) in twice-distilled water was lyophilised in order to remove crystal water. The residue was treated with 1:1 pyridine–acetic anhydride and the resulting octa-acetate was converted into ($^2H_3$)methyl β-cellobioside[12], using an excess of $Hg(CN)_2$ as the promoter. Compound **3** was used to reduce t_1 noise in the 2D NMR spectra caused by overlap of the strong MeO signal with that of H-3.

NMR spectroscopy.—Prior to ^{1}H-NMR spectroscopy, **1–3** were each dissolved in water and the solutions were lyophilised in order to remove crystal water. All experiments were carried out at 500 MHz on a Bruker AM-500 spectrometer interfaced with an Aspect 3000 computer (Department of NMR Spectroscopy, Utrecht University). The processing of the 1D and 2D NMR spectra was performed on a μVAX/VMS-Cluster using the TRITON 2D–3D NMR software package (R. Boelens and R. Kaptein, Department of NMR Spectroscopy).

(a) Solutions in Me_2SO-d_6. 1D ^{1}H-NMR spectra of 10 mM solutions of **1** and **2** in 100.0% Me_2SO-d_6 were recorded at 19°, and from 22 to 42° with increments of 5°, using routine techniques. Resolution enhancement of the spectra was achieved by Lorentzian-to-Gaussian transformation. A homonuclear Hartmann–Hahn (HOHAHA) 2D NMR spectrum was recorded at 27°, using an 80-ms MLEV-17 pulse sequence[13] with a field strength of 9300 Hz. Chemical shifts (δ) are expressed in ppm and referenced to internal sodium 4,4-dimethyl 4-silapentane-1-sulphonate (DSS). The time-proportional phase increment (TPPI) method was used for t_1 amplitude modulation[14–16]; 500 free induction decays (FIDs) of 4096 data points, 8 scans each, were collected. The t_1 period was incremented from 83.3 μs to 83.58 ms. The spectral width was 2994 Hz in each dimension. The time-domain data in each dimension were weighted with a sine-bell function shifted by $\pi/3$. The data were processed to give a phase-sensitive spectrum of 1024 × 2048 data points with a digital resolution of 2.92 Hz/point in the ω_1 domain and 1.46 Hz/point in the ω_2 domain.

(b) Solutions in H_2O–CD_3OD. The NMR spectra of 50 mM solutions of **2** in 4:1 (w/w) H_2O–CD_3OD were acquired at −15 to −6° with increments of 1° at pH 7.0. The addition of CD_3OD up to 20% depresses[17] the freezing point by 15°. The semi-selective pulse sequence[18] 90°–τ–90°–45°–2τ–90°–2τ–45°, wherein the waiting time τ, to adjust the width of the excitation profile, was set to 350 μs, with the carrier positioned at the water resonance, was used to excite the spectral

regions on both sides of the water line except for the solvent protons. Resolution enhancement of the spectra was achieved by Lorentzian-to-Gaussian transformation. Chemical shifts are expressed in ppm and referenced to internal DSS by relation to internal acetone (δ2.225).

NOHOSS 2D NMR spectroscopy.—A build-up series of 2D NOE HOHAHA NMR spectra with semi-selective solvent suppression (NOHOSS)[11] was acquired for a solution of **3** in 4:1 (w/w) H_2O–CD_3OD at pH 6.8 and ~10°. The pulse sequence used was $90°-t_1-90°-\tau_m-90°-SL-\tau-90°-[45°-2\tau-90°-2\tau-45°]_{Ex.}$-Acq($t_2$), wherein τ_m is the NOESY mixing time of 0, 25, 50, 100, or 150 ms. In each experiment, SL was a 20-ms MLEV-17 spin-lock pulse[13] with a field strength of 9400 Hz and τ a constant waiting time of 350 μs. An 8-pulse phase program was applied, which included the suppression of axial peaks and an Exorcycle[19], denoted *Ex.* in the foregoing pulse sequence, for optimal effect of the refocussing pulses. A 90° phase difference between the 3rd 90° pulse and the spin-lock pulses was kept at all times. The carrier frequency was placed on the water resonance. The spectral width was 2994 Hz in each dimension. Spectra were measured in the phase-sensitive mode, using quadrature detection in t_2, and time-proportional phase increments (TPPI)[14–16] to create amplitude modulation in t_1. Every 3rd and 4th experiment, the 4th 90° pulse was given a 180° phase shift. For each NOHOSS experiment, 400 FIDs of 2048 data points, 16 scans each, were collected. The t_1 period was incremented from 83.3 μs to 66.88 ms.

The data in the t_2 domain were multiplied with a $\pi/2$ phase shifted sine-bell function prior to Fourier transformation (FT). A polynomial baseline correction was applied separately on each side of the water line, fitted only on selected empty regions of the spectrum. The data in the t_1 domain were zero-filled and multiplied with a $\pi/2$ phase-shifted sine-bell function prior to phase-sensitive FT, yielding a 1024×512 matrix of real data. A second polynomial baseline correction was applied on records in the ω_1 domain in order to ensure a flat baseplane suitable for accurate cross-peak integration. Peak integration was accomplished by simple summation of intensity in an area around the centre of the peak.

Processing of NOHOSS 2D data.—The processing of NOHOSS intensities is not trivial. Although the technical details of this experiment have been published[11], the processing of the data has not yet been discussed. The NOHOSS pulse sequence consists of two mixing periods, an NOE period followed by a MLEV-17 spin-lock period. Therefore, 3 types of cross-peaks are recognised: type *a* is the pure NOE cross-peak, type *b* is the pure HOHAHA cross-peak, and type *c* is the NOE HOHAHA cross-peak for magnetisation transferred by both mixing sequences. Type *b* cross-peaks contain chemical-shift-correlation information and have been used for assignments. All peak intensities were corrected for non-uniform excitation due to the solvent suppression technique, and for the decrease of total magnetisation caused by relaxation, by normalisation at each mixing time. Normalisation is achieved by relating all peaks in a column (ω_2 constant) to the sum of all intensities in that column.

For quantitative analysis, type *a* cross-peak intensities were also corrected for exchange during spin locking (ROESY type). The normalised type *a* cross-peak intensity is the sum of the transfer probability of NOE mixing and the transfer probability of the spin-lock mixing multiplied by the remainder of the diagonal intensity after NOE mixing. The cross-peak intensity is expressed in eq. *1*,

$$I_{ij}(\tau_m) = P_{ij}^{NOE}(\tau_m) + P_{ij}^{ROE} \cdot \left(1 - P_{ij}^{NOE}(\tau_m)\right) \quad (1)$$

wherein $P_{ij}^{NOE}(\tau_m)$ is the NOE transfer probability as a function of τ_m and P_{ij}^{ROE} is the NOE transfer probability during the constant spin-lock period. The normalised diagonal intensity is then the product of the complements of both transfer probabilities.

$$I_{ii}(\tau_m) = \left(1 - P_{ij}^{NOE}(\tau_m)\right) \cdot \left(1 - P_{ij}^{ROE}\right) \quad (2)$$

The value of P_{ij}^{ROE} is obtained experimentally from the $\tau_m = 0$ experiment. Substitution of the τ_m independent values P_{ij}^{ROE} in eqs. *1* and *2* yields corrected normalised intensities [$I_{ii}^*(\tau_m)$ and $I_{ij}^*(\tau_m)$] that are identical to the NOE transfer probabilities and its complement, respectively. The cross-peak intensities $I_{ij}^*(\tau_m) = P_{ij}^{NOE}(\tau_m)$ were fitted to the exponential function

$$I_{ij}^*(\tau_m) = 1 - c1 \cdot \exp(-c2 \cdot \tau_m). \quad (3)$$

wherein $c1$ and $c2$ are constants to be optimised in the fit procedure. The value of $c1$ should be close to unity due to the normalisation procedure. However, deviating $c1$ values may be obtained when cross-peak intensities are influenced by a systematic offset. The value of k_{ex} is equal to the slope of this function at $\tau_m = 0$, which is the first derivative of eq. *3* to τ_m (i.e., $c1 \cdot c2$).

Quantitative analysis of real NOE HOHAHA cross-peaks (type *c*) reveals k_{ex} of overlapping hydroxyl protons. Magnetisation transferred from the solvent to a type *a* cross-peak with a hydroxyl proton is transferred further to a skeleton proton during the HOHAHA mixing. The efficiency of this transfer is identical to that of the transfer of the hydroxyl diagonal magnetisation to the skeleton proton (type *b* cross-peak). The initial build-up rate of the type *c* cross-peak relative to the sum of the type *c* and *b* cross-peaks is k_{ex}. The type *b* and *c* cross-peaks are treated as the diagonal and type *a* peaks, respectively, in the determination of k_{ex} from the type *a* cross-peaks. The quantification of k_{ex} from the type *c* build-up curves is done by a least-squares fit to eq. *3*. Unlike the easy analysis of the of type *a* cross-peaks, a simple correction for ROESY-type exchange on type *c* cross-peaks will often be impossible, due to low signal-to-noise peaks at $\tau_m = 0$. The effect of ROESY-type exchange can then be estimated by comparing k_{ex} calculated from type *a* and *c* cross-peaks.

Computational details of molecular dynamics simulations.—The MD simulations on methyl β-cellobioside were performed using the program GROMOS[20] and its standard force field for carbohydrates[21]. For water, the SPC model[22] was used. The atomic numbering is shown in Fig. 1 and the atom types and charges, and the

TABLE I

Atom types and partial charges used in GROMOS [20] MD calculations

Atom	Atom type	Charge (*e*) [a]
C-2,3,5,2′,3′,4′,5′	CS1	0.15
C-4	CS1	0.17
C-7	CH3	0.17
C-6,6′	CS2	0.15
C-1,1′	CS1	0.40
O-2,3,6,2′,3′,4′,6′	OA	−0.55
HO-2,3,6,2′,3′,4′,6′	HO	0.40
O-1,5,1′,5′	OS	−0.36
O-W	OW	−0.82
H-W-1,2	HW	−0.41

[a] Each C–O–HO group forms a charge group. In the anomeric region, C-5–O-5–C-1–O-1–C-7 and C-5–O-5′–C-1′–O-1′–C-4 each form a charge group.

charge groups used, are listed in Table I. The united-atom approach for the Lennard-Jones interactions was used for aliphatic carbon atoms. The methyl β-cellobioside molecule was placed in a periodic computational box: a truncated octahedron containing 358 water molecules. A cut-off radius for non-bonded interactions, based on charge groups for electrostatic interactions, of 8.0 Å was used. After initial energy minimisation of the whole system, the MD simulations were performed[23] at a constant pressure of 1 atm with a relaxation time of 0.5 ps, and at a constant temperature of 27° by loose coupling to a temperature bath with a relaxation time of 0.1 ps. The time step was 0.002 ps. All bond lengths were constrained and the water molecules were kept completely rigid by using the SHAKE method[24]. A non-bonded pair list was updated every 5 MD steps. The first 10 ps of each run were considered to be the equilibration time. After that, data were stored every 10 MD steps. Three separate runs of 100 ps each were performed: (*a*) both hydroxymethyl groups were initially placed in the *tg* conformation; (*b*) derived from the configuration of (*a*) after 10 ps, by minimisation and renewed assignment of velocities from a Maxwell distribution; and (*c*) both hydroxymethyl groups in the *gt* conformation. Many transitions of both hydroxymethyl groups occurred so that the choice of the starting conformations is not important. The runs (*a*)–(*c*) were each performed in a (ϕ, ψ) range that is normal for the crystal structures of cellulose, methyl β-cellobioside, and cellobiose[25,26]. Additional (ϕ, ψ) conformations (See Fig. 1) were simulated, but are considered to be less important[27,28]. The calculations were performed on the local μVAX/VMS cluster.

All data were averaged over 300 ps. The fraction of time an intramolecular hydrogen bond exists was evaluated by counting the number of time steps in which HO $\cdots$ O_{intra} was < 2.4 Å. (*a*) The donor and acceptor capacity of hydroxyl groups are expressed by the fraction of time that HO $\cdots$ O-W of < 2.4 Å holds for the donors, and that O $\cdots$ H-W of < 2.4 Å holds for the acceptors. The suffix W indicates that the atom is part of a solvent molecule. These two capacities are

summed to give $D+A$ which is a measure of the interaction with nearby water molecules. (*b*) The radial distribution function $g(r)$ for each solute atom X to solvent atom W is given[29] by

$$g_{X\cdots W}(r) = \langle N_{X\cdots W}(r)\rangle / N_{ran}(r), \quad (4)$$

where $\langle N_{X\cdots W}(r)\rangle$ is the actual number of pairs X $\cdots$ W at distance r and $N_{ran}(r)$ is the same number from a random distribution. Only atoms W in the primary solvation of atom X are considered. The primary solvation of atom X is defined[29] as the volume in which atoms W are nearer to atom X than to any other atom in the methyl β-cellobioside molecule. The $g(r)$ functions for HO $\cdots$ O-W and O $\cdots$ H-W are calculated. Integration of $\langle N_{X\cdots W}(r)\rangle$ yields the cumulative distribution function giving the running co-ordination number at distance r_c:

$$C_{X\cdots W}(r_c) = \int_0^{r_c} \langle N_{X\cdots W}(r)\rangle \, dr \quad (5)$$

The running co-ordination numbers for each hydroxyl group $C_s(r_c)$ at 2.4 Å were obtained from $C_s(2.4) = C_{HO\cdots O\text{-}W}(2.4) + C_{O\cdots H\text{-}W}(2.4)$. (*c*) Solvent-accessible surfaces were calculated with the MS program[30] using a static molecular model. Because the hydroxyl hydrogen atoms take many different positions during the simulations, the hydrogen atoms were removed and the co-ordinates of the C and O atoms were averaged over 100 ps by fitting the ring atoms at every time step by least squares. Subsequently, the hydroxymethyl groups were placed once each in the *gt* and *gg* conformation. From these models, the average surface of the methyl β-cellobioside molecule with a known experimental distribution[27] of the *gg* and *gt* conformations was calculated. The surface was then subdivided into parts belonging to each atom to which it is closest. The surface of the O atom is regarded representative of the hydroxyl group. A probe radius of 1.5 Å and a van der Waals radius of 2.4 Å for both C and O was used. (*d*) The average interaction energy with all water molecules, within a cut-off radius of 8 Å, was calculated for each charge group (C–O–HO) to which a hydroxyl group belongs. (*e*) Each primary solvation can be subdivided in the 1st, 2nd, and possibly 3rd shell, of which only the 1st is used. For H $\cdots$ O interactions, the 1st shell ends at 2.4 Å which corresponds to the first minimum in the radial distribution function. The residence time of water molecules τ_r in the 1st shell of a hydroxyl group is obtained from the following relation[31]:

$$NP(\Delta t) = \frac{1}{N_{dat}} \sum_{k=1}^{N_{dat}} \sum_{j=1}^{N_{sm}} P_j(t_k, \Delta t, t^*) = NP(0) \cdot \exp(-\Delta t/\tau_r) \quad (6)$$

where $P_j(t_k, \Delta t, t^*) = 1$ if the water molecule j is in the 1st shell at time t_k and at $t_k + \Delta t$, whilst it has not been out of the shell during Δt, for any continuous period longer than t^*, which was set to 2 ps in this study; $P_j = 0$ otherwise.

$$NP(0) = \frac{1}{N_{dat}} \sum_{k=1}^{N_{dat}} \sum_{j=1}^{N_{sm}} P_j(t_k, 0, 0) \quad (7)$$

which gives the average number of water molecules in the 1st shell. The parameter τ_r is determined by a least-squares fit of eq. *6* similar to the procedure described[31]. Index k runs over the number of data, being N_{dat} time steps, and j runs over the total number of water molecules, N_{sm}. $NP(\Delta t)$ is a time-correlation function which can be fitted to an exponential curve by least-squares. (*f*) A quantity related to τ_r and $NP(0)$ is the average time spent by a water molecule in the 1st shell:

$$t_s = \sum_{k=1}^{N_{dat}} \sum_{j=1}^{N_{sm}} P_j(t_k, 0, 0) \cdot t_{step}/N_{wat} \qquad (8)$$

where N_{wat} is the number of different water molecules visiting the shell during N_{dat} time steps t_{step}. $NP(0)$ is the average number of water molecules in the 1st shell, whereas t_s is the average time spent in the 1st shell by these water molecules ($= N_{dat} \cdot t_{step} \cdot NP(0)/N_{wat}$). (*g*) The average number of times that the N_{wat} water molecules enter the 1st shell of a hydroxyl group during a given simulation time is called N_{occur}.

RESULTS AND DISCUSSION

1D NMR spectroscopy on solutions in Me_2SO-d_6.—The ^{1}H-NMR signals of a solution of **1** in Me_2SO-d_6 could be assigned directly by measurement of the ^3J values. The complete ^{1}H-NMR assignment for a solution of **2** in Me_2SO-d_6, given in Table II and derived from the HOHAHA experiment, matches an earlier assignment[8], provided that an offset of 0.117 ppm is taken into account because of a different spectral calibration. In order to determine the $d\delta/dT$ values of the hydroxyl protons quantitatively, the measured values were fitted to a straight line by a least-squares method. The temperature dependences of the chemical shifts of the resonances of the hydroxyl protons of **1** and **2** are shown graphically in Fig. 2 and listed as $d\delta/dT$ values in Table III. From the relatively low coefficient (< 3 ppb/deg) for HO-3 in **2** and from its small $^3J_{HO,CH}$ (1.7 Hz), which indicates H–O–C–H θ to be $\sim 90°$ with little rotational freedom, the existence of an HO-3 $\cdots$ O-5′ intramolecular hydrogen bond is inferred. Similar behaviour has been found for solutions of several β-(1 → 4)-linked carbohydrates dissolved in Me_2SO or other aprotic solvents[8,10,33–36]. The upfield shift of the resonance of the intramolecularly hydrogen-bonded HO-3 in solution in Me_2SO-d_6 relative to those of the resonances of the other hydroxyl protons contrasts with the general observation that the resonances of the intramolecularly hydrogen-bonded protons are shifted downfield. The chemical shifts, however, are subject to numerous other influences, and are therefore unreliable.

1D NMR spectroscopy on solutions in H_2O–CD_3OD.—An intriguing question is whether the HO-3 $\cdots$ O-5′ intramolecular hydrogen bond survives in a protic solvent such as water. The resonances of hydroxyl protons cannot be observed at

TABLE II

Assignments of ^1H resonances (ppm) for methyl β-D-glucopyranoside (**1**), methyl β-cellobioside (**2**) for solutions in Me_2SO-d_6, and ($^2H_3$)methyl β-cellobioside (**3**) for a solution in 4:1 (w/w) H_2O–CD_3OD

Residue	Atom	1	2	3
Reducing end	H-1	4.053	4.124	4.394
	H-2	2.961	3.034	3.285
	H-3	3.153	3.335	3.626
	H-4	3.059	3.3 [b]	3.639
	H-5	3.108	3.287	3.585
	H-6*proS*	3.696	3.774	3.998
	H-6*proR*	3.465	3.644	3.836
	HO-2	5.046	5.177	6.727
	HO-3	4.935 [a]	4.680	5.966
	HO-4	4.915 [a]		
	HO-6	4.522	4.613	5.952
Non-reducing end	H-1′		4.278	4.487
	H-2′		3.020	3.303
	H-3′		3.183	3.491
	H-4′		3.078	3.400
	H-5′		3.209	3.465
	H-6′*proS*		3.722	3.922
	H-6′*proR*		3.432	3.737
	HO-2′		5.240	6.683
	HO-3′		5.022	6.556
	HO-4′		4.995	6.448
	HO-6′		4.599	6.133

[a] Values may be interchanged. [b] No accurate value, due to severe overlap.

room temperature in aqueous solutions. However, continuous wave (CW) measurements at sub-zero temperatures and at high concentrations of carbohydrates showed that the exchange rates of sugar hydroxyl protons were low enough to give rise to well-resolved resonances[37]. The 1D ^1H-NMR spectrum of a solution of **2** in H_2O–CD_3OD at $-10°$ is shown in Fig. 3. The opposite signs of the signals on both sides of the water line are caused by the semi-selective excitation technique used to eliminate the water signal. The assignment of the proton resonances was derived from the NOHOSS spectrum[11], which contains chemical-shift correlation information like a HOHAHA spectrum, and is listed in Table II. The $d\delta/dT$ values of the hydroxyl protons listed in Table III are quantified by a least-squares fit of the experimental chemical shifts to a straight line as a function of temperature, as shown graphically in Fig. 4. Since no hydroxyl proton resonance exhibits a deviating temperature dependence, it is concluded that no dominant intramolecular hydrogen bond exists in **2** in the H_2O–CD_3OD solvent system.

The $^3J_{HO,CH}$ value for HO-3 cannot be determined accurately due to the almost complete overlap of the signals of HO-3,6. Only after extreme sharpening of the lines by Lorentzian-to-Gaussian transformation (LB = −3.0, GB = 0.4), the J value was estimated to be ~3 Hz. Although not large, this value is significantly

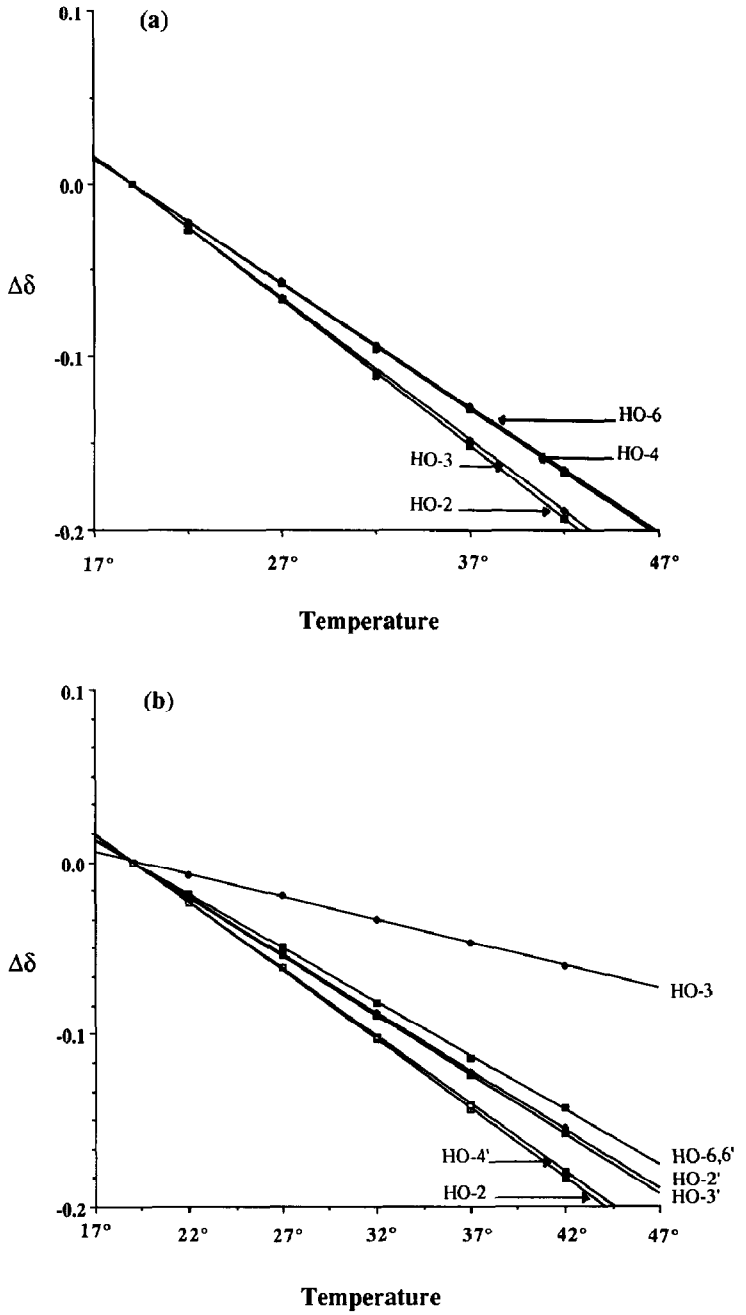

Fig. 2. Temperature dependence of hydroxyl proton resonances of (a) methyl β-D-glucopyranoside (**1**) and (b) methyl β-cellobioside (**2**) in solution in Me_2SO-d_6.

higher than the corresponding value (1.7 Hz) of **2** in solution in Me_2SO-d_6, thereby further indicating that the average orientation of HO-3 is not restricted to 90° and therefore does not favour intramolecular hydrogen bonding.

TABLE III

$d\delta/dT$ Values (ppm/deg) for methyl β-D-glucopyranoside (**1**) and methyl β-cellobioside (**2**) in solution in Me_2SO-d_6, and ($^2H_3$)methyl β-cellobioside (**3**) in solution in 4:1 (w/w) H_2O–CD_3OD

Residue	Atom	1	2	3
Reducing end	HO-2	8.4	8.0	12.2
	HO-3	8.2	2.6	11.1
	HO-4	7.3		
	HO-6	7.2	6.3 [a]	12.3
Non-reducing end	HO-2′		6.8	10.7
	HO-3′		6.9	11.5
	HO-4′		7.8	10.6
	HO-6′		6.3 [a]	12.7

[a] Average value due to overlap.

NOHOSS 2D NMR spectroscopy on solutions in H_2O–CD_3OD.—NOHOSS[11] spectroscopy was used because k_{ex} for HO-3 in **3** in solution in H_2O–CD_3OD cannot be determined uniquely by NOESY, due to overlap with the HO-6 resonance. In the NOHOSS[11] experiment, the exchange effects of the overlapping HO-3,6 resonances can be observed at the resonance frequencies of the adjacent skeleton atoms H-3, H-6*proS*, and H-6*proR*, respectively. The intensities of the type *a* peaks were normalised and corrected for exchange during the spin-lock

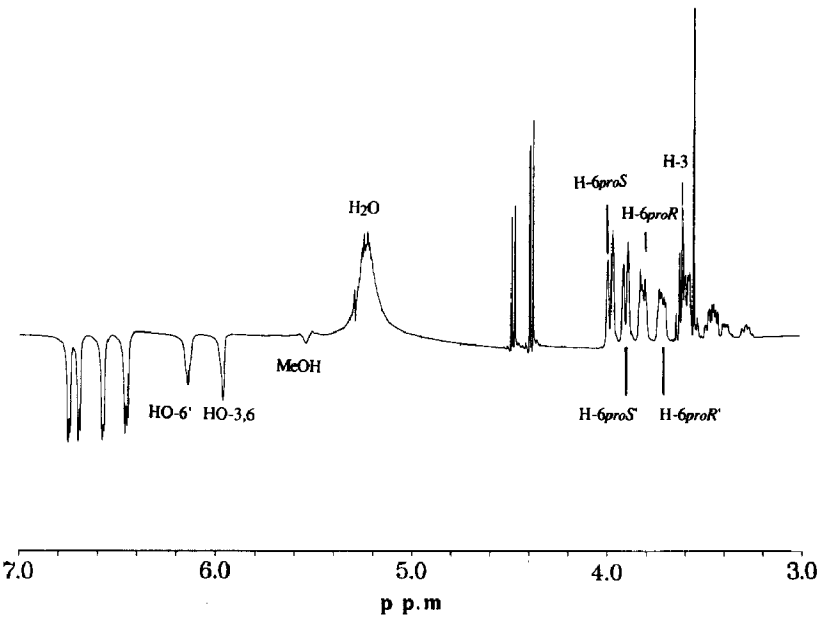

Fig. 3. ^{1}H-NMR spectrum (500 MHz) of methyl β-cellobioside (**2**) in 4:1 (w/w) H_2O–CD_3OD at −10° (the non-uniform excitation is caused by a semi-selective excitation pulse used to suppress the water signal).

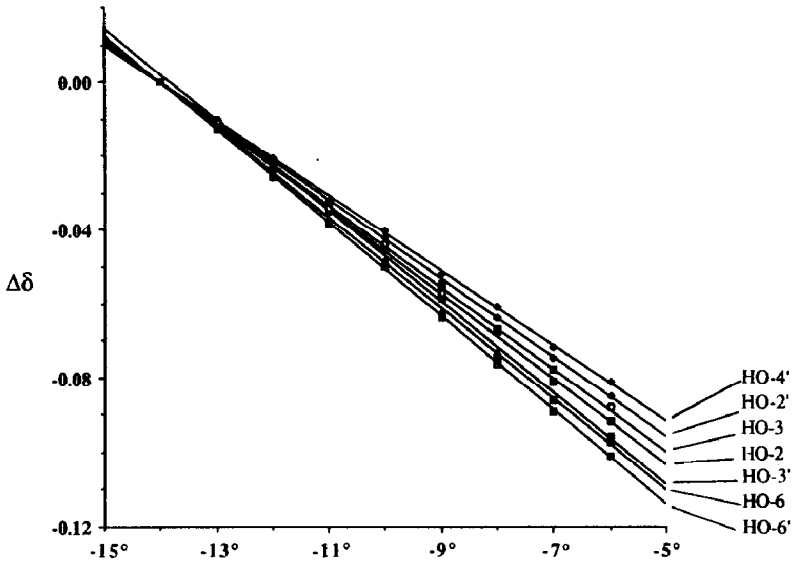

Fig. 4. Temperature dependence of hydroxyl proton resonances of a methyl β-cellobioside (2) solution in 4:1 (w/w) H_2O–CD_3OD.

period. Almost perfect build-up curves were obtained for these pure exchange cross-peaks between the hydroxyl protons and water as shown in Fig. 5a. The values of k_{ex} derived from these curves are listed in Table IV and average values were calculated for HO-3,6. In order to resolve the problem of overlap, the normalised type *c* cross-peaks were analysed and related to the type *b* (pure HOHAHA) cross-peaks. Although the resulting build-up curves, as shown in Fig. 5b, measured at the four H-6 resonances are less ideal than those for the pure exchange cross-peaks between hydroxyl protons and water, accurate values for k_{ex} could be obtained by fitting the data points to eq. *3*. Since the excitation profile of the NOHOSS experiments was tuned on the H-6 signals, low intensities and low signal-to-noise ratios were obtained for cross-peaks of protons in the bulk region of the spectrum, which are therefore not accessible for calculations. The individual values of k_{ex} for HO-6,6′ can be calculated easily as the average of the initial build-up rates H-6*proS* and H-6*proR*, and H-6′*proS* and H-6′*proR*, respectively. The accuracy of the technique was checked by comparison of the two k_{ex} values for HO-6′, namely from the direct NOE peak with water and from the relayed H-6′*proS* and H-6′*proR* data. The latter k_{ex} value was slightly higher. This result was expected since no correction was applied for exchange in the rotating frame. The ROESY-type exchange appears to increase the calculated rate by ~ 10%, as shown in Table IV. It was not possible to correct for this type of magnetisation transfer before calculation of the rates, because the intensities of the cross-peaks

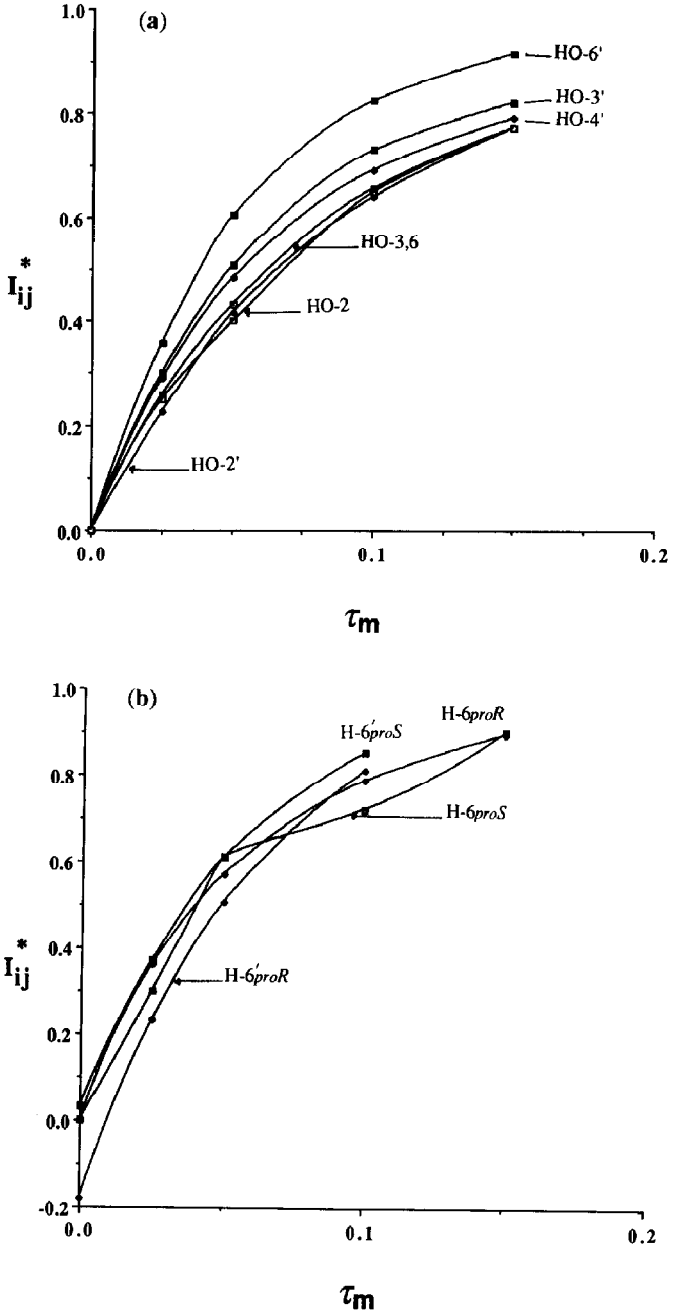

Fig. 5. Build-up curves for the chemical exchange between hydroxyl protons and water of a ($^2H_3$)methyl β-cellobioside (3) solution in 4:1 (w/w) H_2O–CD_3OD caused by longitudinal exchange only: (a) pure NOE and (b) relayed NOE curves.

between the water and the skeleton protons in the $\tau_m = 0$ experiment were too low to give reliable integral values. The calculated rate for HO-6 was decreased by 10% to compensate for the exchange during spin locking. The small coupling

TABLE IV

Hydroxyl proton k_{ex} values (s^{-1}) for ($^2H_3$)methyl β-cellobioside (3) in solution in 4:1 (w/w) H_2O–CD_3OD. Type *a* values are derived from pure NOE cross-peaks

Residue	Atom	Type *a*	Type *c* [a]	Combined type *a* and *c*
Reducing end	HO-2	9.9		
	HO-3	10.0 [b]		6.7 [c]
	HO-6	10.0 [b]	14.8	13.3 [c]
Non-reducing end	HO-2′	9.9		
	HO-3′	11.6		
	HO-4′	10.4		
	HO-6′	16.6	18.8	16.6

[a] Type *c* values are derived from NOE HOHAHA cross-peaks. [b] Averaged values, due to severe overlap. [c] Type *c* values after correction by 10%, similar to the effect of ROESY transfer measured for HO-6′ (see text).

between HO-3 and H-3 gives rise to low signal-to-noise cross-peaks and also between H-3 and water, due to slow HOHAHA type transfer. Additionally, the line shape of the H-3 resonance was distorted, due to strong coupling with H-4 and H-5 that resonate at frequencies close to that of H-3. Therefore, the resulting build-up curve could not be used for quantitative analysis. However, the k_{ex} value for HO-3 was calculated from the known average value for HO-3 and HO-6, in combination with the known k_{ex} of HO-6, and is listed in Table IV. This results in a value that is lower than that of any other exchange rate.

MD simulations.—Simulations for an aqueous solution of methyl β-cellobioside can give additional information. All parameters obtained from analyses (*a*)–(*g*) were calculated for the seven hydroxyl groups. The main focus is on the occurrence of the HO-3 · · · O-5′ hydrogen bond. Its absence in a solution in H_2O–CD_3OD is suggested by the $d\delta/dT$ value for HO-3, which does not differ significantly from those of the other hydroxyl protons. When using the criterion HO · · · O < 2.4 Å, the HO-3 · · · O-5′ hydrogen bond exists for 29% of the time. Although this criterion is arbitrary, since it is based on the 1st minimum in the radial distribution function, this percentage indicates that this particular intramolecular hydrogen bond is not pronounced. In contrast, the low k_{ex} value for HO-3 in the same solvent system seems to indicate a distinct behaviour. It cannot be concluded whether the low HO-3 k_{ex} is caused by the 29% of intramolecular hydrogen bonding, or whether other intermolecular processes play an important role. Therefore, further analysis is necessary in order to determine the cause(s) of the variations of $d\delta/dT$ and k_{ex}.

The parameters obtained from analyses (*a*)–(*g*) are plotted in Figs. 6 and 7 against $d\delta/dT$ and k_{ex}, respectively. The corresponding Spearman rank-order correlation coefficients R_s and Kendall's τ (ref. 32), and their significance, are listed in Table V. For $d\delta/dT$, a convincing correlation was found with the average interaction energy $E(d)$ with water of each hydroxyl group ($R_s = -0.99$), as shown

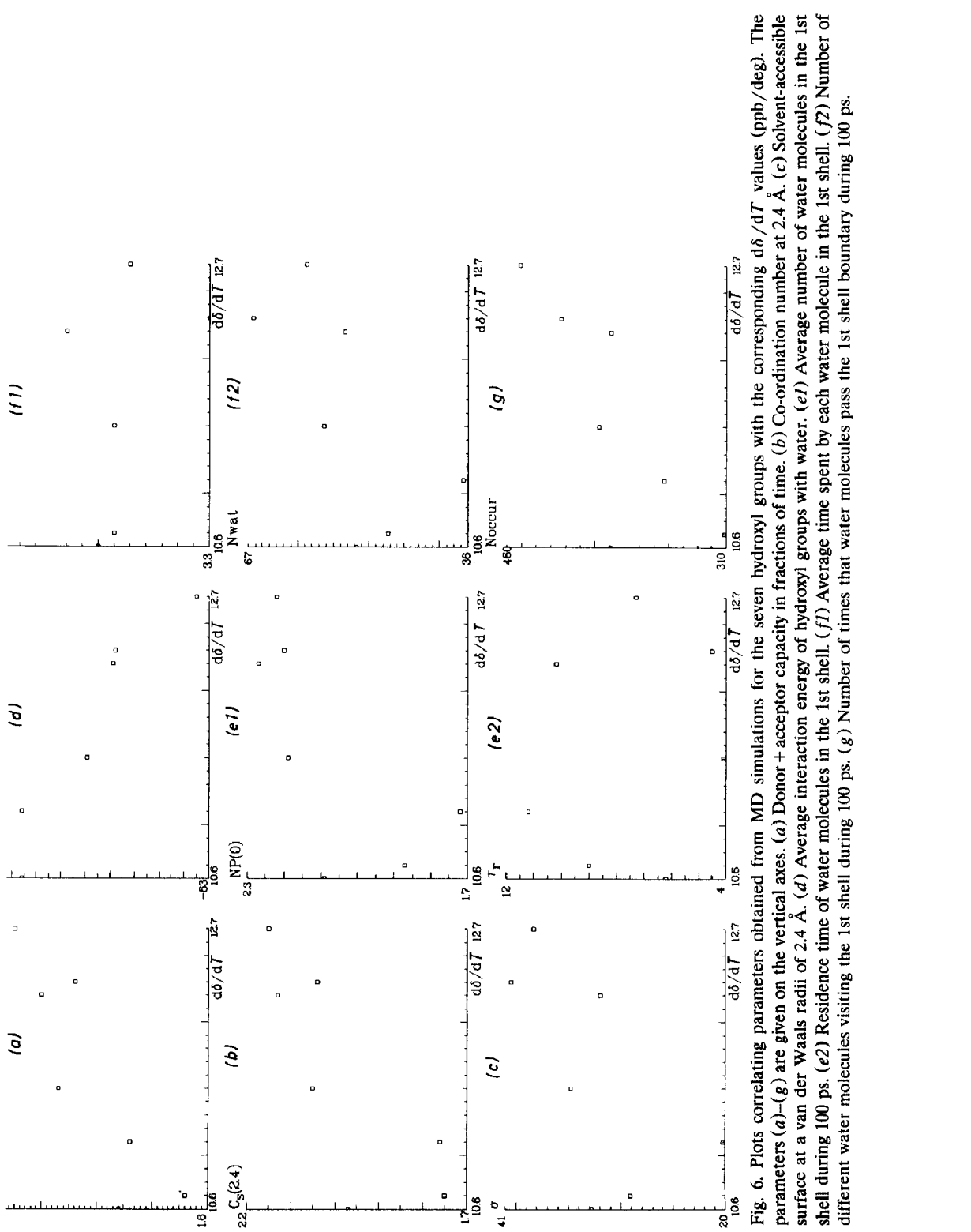

Fig. 6. Plots correlating parameters obtained from MD simulations for the seven hydroxyl groups with the corresponding $d\delta/dT$ values (ppb/deg). The parameters (*a*)–(*g*) are given on the vertical axes. (*a*) Donor + acceptor capacity in fractions of time. (*b*) Co-ordination number at 2.4 Å. (*c*) Solvent-accessible surface at a van der Waals radii of 2.4 Å. (*d*) Average interaction energy of hydroxyl groups with water. (*e1*) Average number of water molecules in the 1st shell during 100 ps. (*e2*) Residence time of water molecules in the 1st shell. (*f1*) Average time spent by each water molecule in the 1st shell. (*f2*) Number of different water molecules visiting the 1st shell during 100 ps. (*g*) Number of times that water molecules pass the 1st shell boundary during 100 ps.

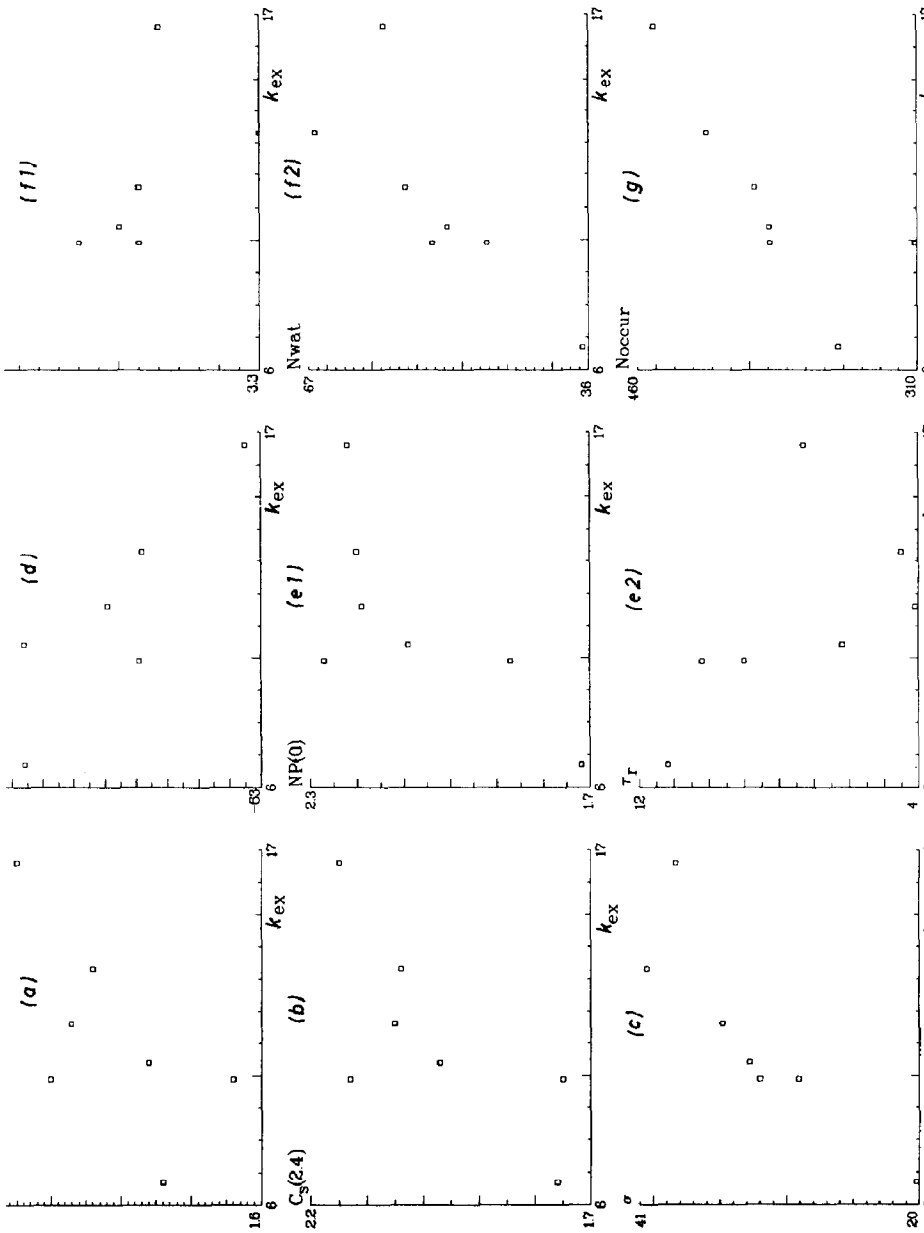

Fig. 7. Plots correlating parameters obtained from MD simulations for the seven hydroxyl groups with the corresponding k_{ex} values (s^{-1}). The parameters (*a*)–(*g*) are given on the vertical axes and are explained in Fig. 6.

TABLE V

Correlation coefficients [a] of MD and NMR data

	$d\delta/dT$		k_{ex}	
	R_s (s)	τ (s)	R_s (s)	τ (s)
(*a*) $D+A$	0.79 (0.04)	0.62 (0.05)	0.59 (0.16)	0.49 (0.12)
(*b*) $C_s(2.4)$	0.79 (0.04)	0.62 (0.04)	0.59 (0.16)	0.49 (0.12)
(*c*) σ	0.64 (0.12)	0.43 (0.18)	0.92 (0.01)	0.89 (0.01)
(*d*) E	−0.99 (0.00)	−0.88 (0.01)	−0.85 (0.02)	−0.65 (0.04)
(*e*) $NP(0)$	0.75 (0.05)	0.52 (0.10)	0.52 (0.23)	0.59 (0.06)
τ_r	−0.14 (0.75)	−0.05 (0.88)	−0.79 (0.03)	−0.59 (0.06)
(*f*) t_s	−0.59 (0.16)	−0.39 (0.22)	−0.97 (0.00)	−0.75 (0.02)
N_{wat}	0.78 (0.04)	0.52 (0.10)	0.86 (0.01)	0.78 (0.01)
(*g*) N_{occur}	0.71 (0.07)	0.62 (0.05)	0.90 (0.01)	0.88 (0.01)

[a] The correlation coefficients can take values in the range −1 to 1: a value of 1 or −1 means that the data are fully correlated, whereas a value of 0 means that no correlation has been found. The brackets contain the significance s of the R_s or τ value, i.e., the probability that a random distribution is actually random. Correlation between 0 and 1.

in Fig. 6d. To a lesser extent, a positive correlation with the co-ordination numbers $C(2.4)$ (*b*) and $D+A$ (*a*) was found, which are also related to the interaction with the solvent. Thus, the stronger the interaction of the hydroxyl group with the solvent, the larger is the influence of the temperature on the chemical shift, as noted in the Introduction. Fig. 8 shows that there is no strong correlation between $d\delta/dT$ and k_{ex} and indicates that they reflect essentially different parameters. For k_{ex}, three parameters, $t_s(f)$, σ (*c*), and N_{occur} (*g*), have correlation coefficients $|R_s| > 0.90$ and $|\tau| > 0.75$. The most extreme data points in k_{ex} were found for HO-3 and O-3. In order to understand the above correlations, $g(r)$ of HO-3 · · · O-W and O-3 · · · H-W must be compared to the averaged $g(r)$ of HO · · · O-W and O · · · H-W of the six other hydroxyl groups, and are shown in Fig. 9 At first sight the $g(r)$ for O-3/HO-3 and O/HO differ only in the amount of noise, and the same positions for the maxima and minima were found. However, the cumulative distribution $C(r)$ is quite different and leads to a large difference in co-ordination number at 10.0 Å. Hence, there is a difference in $g(r)$ which accumulates at larger

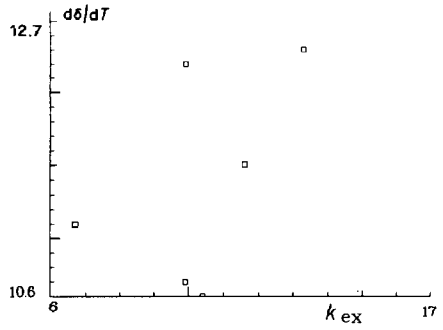

Fig. 8. Plot of $d\delta/dT$ against k_{ex}.

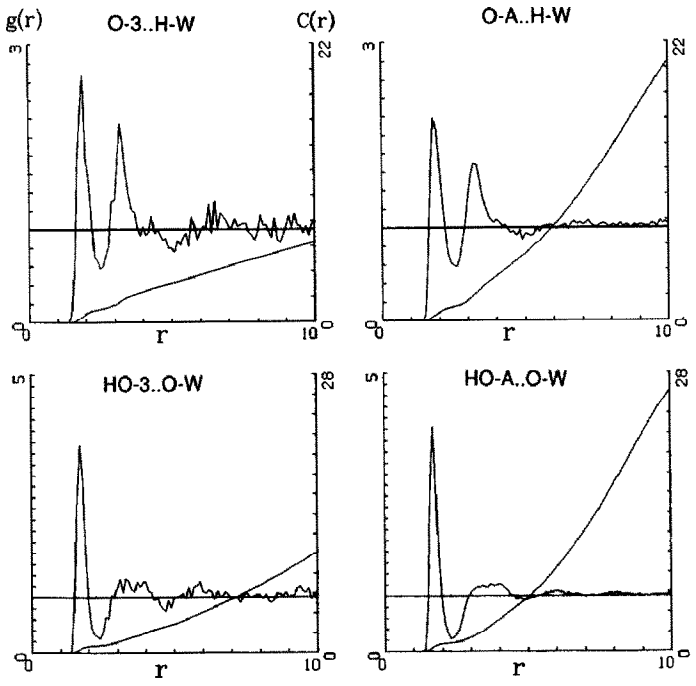

Fig. 9. Radial distribution functions $g(r)$ (left y axis) and cumulative distribution functions $C(r)$ (right y axis) for H · · · O distances. O-A · · · H-W indicates the average distributions for all hydroxyl group O to water H interactions (except O-3 · · · H-W), and HO · · · O-W indicates the averaged hydroxyl H to water O interactions (except HO-3 · · · O-W).

distances. The amount of available volume in the primary solvation is an important factor in determining the co-ordination number. That this effect already exists at 2.4 Å is shown in Fig. 7b where $C_s(r_c)$ at 2.4 Å is plotted against k_{ex}. Moreover, O-2′/HO-2′ also has a small co-ordination number. These findings prompts the evaluation of the parameters (*c*)–(*g*). *NP*(0) (*e*) is also a measure of the volume of the 1st shell and, indeed, its correlation plot (Fig. 7e1) strongly resembles that of $C_s(2.4)$ (*b*). However, the correlation coefficients R_s and τ are not sufficiently reliable. The best (inverse) correlation is found with the average time spent in the 1st shell $t_s(f1)$ and, to a lesser extent, with the residence time τ_r (*e*2), which are measures of the dynamic character of the water molecules in the 1st shell. Apparently, the exchange rate decreases if the water molecules remain in the 1st shell for only a short time. A good correlation was also found with the solvent-accessible surface σ at 2.4 Å (*c*), so that, even more than the volume, the surface of the 1st shell turns out to be determinant. It is likely that t_s and τ_r are affected by the solvent-accessible surface because the larger the surface, the easier the water molecules can enter and leave the 1st shell. This inference suggests that the number of water molecules, N_{occur} (*g*), that enter the 1st shell per unit time determines the exchange rate. This quantity shows a good correlation with k_{ex}. During the 300 ps of simulation, several transitions of both hydroxymethyl groups

occurred and ω' was involved in 16 transitions, all between the *gt* and *tg* conformations, giving a distribution $gg:gt:tg = 0.00:0.74:0.26$. With 14 transitions, the distribution was 0.24:0.51:0.25. The *gg* conformation was visited once for 72 ps. The experimental distribution obtained from the $^3J_{H,H}$ values[27] was 0.52:0.48:0.00 for each hydroxymethyl group. It is clear that the number of conformational transitions is too small to obtain a reliable distribution from the residence times of the three conformations. From longer simulations[28], it was estimated that ~2 ns have to be simulated in order to obtain the correct distributions. In view of the large computational efforts required, these long simulations are not feasible at present. This means that data obtained in the analyses (*a*)–(*g*), that are sensitive to the distribution of the hydroxymethyl group, have to be interpreted with some caution. The plots in Fig. 7 show that the data of (H)O-6 or (H)O-6′ and (H)O-2′ sometimes look like outliers which may be caused by the incorrect conformational distribution of both hydroxymethyl groups. In the *tg* conformation, which should not be present, O-6 comes close to O-2′, so that also the HO-2/O-2′ data can be affected.

Extrapolation of the results for methyl β-cellobioside to cellulose suggests that intramolecular hydrogen bonding does not contribute significantly to the rigidity of cellulose chains during the spinning of fibres from aqueous solutions. Since the rigidity of the molecules affects the regular orientation in fibres, these results indicate that spinning from non-aqueous solutions could result in highly oriented fibres.

ACKNOWLEDGMENTS

We thank Dr. M.G. Northolt and Dr. P. de Waard for valuable suggestions, Drs. R.W.W. Hooft for assistance, and Professor. Dr. W.F. van Gunsteren for the use of the GROMOS program package. This work was supported by the Netherlands Program for Innovation Oriented Carbohydrate Research (IOP-k) with financial aid of the Ministry of Economic Affairs and the Ministry of Agriculture, Nature Management and Fisheries.

REFERENCES

1 R.H. Marchessault and P.R. Sundararajan, in G.O. Aspinall (Ed.), *The Polysaccharides*, Vol. 2 Academic Press, London, 1983, chap. 2.
2 K.H. Gardner and J. Blackwell, *Biopolymers*, 13 (1974) 1975–2001.
3 F.J. Kolpak and J. Blackwell, *Macromolecules*, 9 (1976) 273–278.
4 M.G. Northolt and H. De Vries, *Angew. Makromol. Chem.*, 133 (1985) 183–203.
5 M.G. Northolt and R. Van der Hout, *Polymer*, 26 (1985) 310–316.
6 L.M.J. Kroon-Batenburg, J. Kroon, and M.G. Northolt, *Polym. Commun.*, 27 (1986) 290–292.
7 M. St-Jacques, P.R. Sundararajan, K.J. Taylor, and R.H. Marchessault, *J. Am. Chem. Soc.*, 98 (1976) 4386–4391.
8 D. Gagnaire, J. St-Germain, and M. Vincendon, *J. Appl. Polym. Sci.: Appl. Polym. Symp.*, 37 (1982) 261–275.

9 R. Nardin and M. Vincendon, *Macromol. Chem.*, 189 (1988) 153–162.
10 R.R. Fraser, M. Kaulman, P. Morand, and G. Govil, *Can. J. Chem.*, 47 (1969) 403–409.
11 B.R. Leeflang and J.F.G. Vliegenthart, *J. Magn. Reson.*, 89 (1990) 615–619.
12 F. Smith and J.W. Van Cleve, *J. Am. Chem. Soc.*, 74 (1952) 1912–1913.
13 D.G. Davis and A. Bax, *J. Am. Chem. Soc.*, 107 (1985) 2820–2821.
14 D. Marion and K. Wüthrich, *Biochem. Biophys. Res. Commun.*, 113 (1983) 967–974.
15 G. Drobney, A. Pines, S. Sinton, D. Weitekamp, and D. Werner, *Faraday Symp. Chem. Soc.*, 13 (1979) 49–55.
16 G. Bodenhausen, R.L. Vold, and R.R. Vold, *J. Magn. Reson.*, 37 (1980) 93.
17 R.C. Weast (Ed.), *CRC Handbook of Chemistry and Physics*, 62nd edn., CRC Press, Boca Raton, Florida, 1981, p. D-217.
18 M. von Kienlin, M. Decorps, J.P. Albrand, M.F. Foray, and P. Blondet, *J. Magn. Reson.*, 76 (1988) 169–173.
19 G. Bodenhausen, R. Freeman, and D.L. Turner, *J. Magn. Reson.*, 27 (1977) 511.
20 W.F. van Gunsteren, *GROMOS, Groningen Molecular Simulation Package*, University of Groningen, The Netherlands, 1987.
21 J. Koehler, W. Saenger, and W.F. van Gunsteren, *Eur. Biophys. J.*, 15 (1987) 197–210.
22 H.J.C. Berendsen, J.P.M. Postma, W.F. van Gunsteren, and J. Hermans, in B. Pullmann (Ed.), *Intermolecular Forces*, Reidel, Dordrecht, 1981, pp. 331–343.
23 H.J.C. Berendsen, J.P.M. Postma, W.F. van Gunsteren, A. Dinola, and J.R. Haak, *J. Chem. Phys.*, 81 (1984) 3684–3690.
24 W.F. van Gunsteren and H.J.C. Berendsen, *Mol. Phys.*, 34 (1977) 1311–1327.
25 J.T. Ham and D.G. Williams, *Acta Crystallogr., Sect. B*, 26 (1977) 1373–1383.
26 S.S.C. Chu and G.A. Jeffrey, *Acta Crystallogr., Sect. B*, 24 (1968) 830–838.
27 L.M.J. Kroon-Batenburg, J. Kroon, and M.G. Northolt, *Papier*, 44 (1990) 640–647.
28 L.M.J. Kroon-Batenburg, B.R. Leeflang, J. Kroon, and J.F.G. Vliegenthart, unpublished data.
29 B.P. van Eijck, L.M.J. Kroon-Batenburg, and J. Kroon, *J. Mol. Struct.*, 237 (1990) 315–325.
30 M.L. Connoly, *Molecular Surface Program*, QCPE No. 429, Department of Chemistry, Indiana University, Bloomington, IN 47405, USA.
31 R.W. Impey, P.A. Madden, and I.R. McDonald, *J. Phys. Chem.*, 87 (1983) 5071–5083.
32 W.H. Press, B.P. Flannery, S.A. Tenkolsky, and W.T. Vetterling, *Numerical Recipes*, Cambridge University Press, 1986, pp. 489–494.
33 K.K. Ghosh and R.D. Gilbert, *Text. Res. J.*, 41 (1971) 326–330.
34 F. Heatley, J.E. Scott and B. Casu, *Carbohydr. Res.*, 72 (1979) 13–23.
35 J.E. Scott, F. Heatley, and W. Hull, *Biochem. J.*, 220 (1984) 197–205.
36 M. Vincendon, *Makromol. Chem.*, 186 (1985) 1787–1795.
37 J.M. Harvey, M.C.R. Symons, and R.J. Naftalin, *Nature (London)*, 261 (1976) 435–436.